The Exon Junction Complex and Srp54 Contribute to Hedgehog Signaling via *ci* RNA Splicing in *Drosophila melanogaster*

Elisa Garcia-Garcia,[1] Jamie C. Little,[1] and Daniel Kalderon[2]
Department of Biological Sciences, Columbia University, New York, 10027
ORCID IDs: 0000-0002-3587-0474 (E.G.-G.); 0000-0002-2149-0673 (D.K.)

ABSTRACT Hedgehog (Hh) regulates the Cubitus interruptus (Ci) transcription factor in *Drosophila melanogaster* by activating full-length Ci-155 and blocking processing to the Ci-75 repressor. However, the interplay between the regulation of Ci-155 levels and activity, as well as processing-independent mechanisms that affect Ci-155 levels, have not been explored extensively. Here, we identified Mago Nashi (Mago) and Y14 core Exon Junction Complex (EJC) proteins, as well as the Srp54 splicing factor, as modifiers of Hh pathway activity under sensitized conditions. Mago inhibition reduced Hh pathway activity by altering the splicing pattern of *ci* to reduce Ci-155 levels. Srp54 inhibition also affected pathway activity by reducing *ci* RNA levels but additionally altered Ci-155 levels and activity independently of *ci* splicing. Further tests using *ci* transgenes and *ci* mutations confirmed evidence from studying the effects of Mago and Srp54 that relatively small changes in the level of Ci-155 primary translation product alter Hh pathway activity under a variety of sensitized conditions. We additionally used *ci* transgenes lacking intron sequences or the presumed translation initiation codon for an alternatively spliced *ci* RNA to provide further evidence that Mago acts principally by modulating the levels of the major *ci* RNA encoding Ci-155, and to show that *ci* introns are necessary to support the production of sufficient Ci-155 for robust Hh signaling and may also be important mediators of regulatory inputs.

KEYWORDS Hedgehog signaling; exon junction complex; cubitus interruptus; splicing; *Drosophila*

HEDGEHOG (Hh) signaling plays many roles in development and tissue maintenance from *Drosophila* to humans. Accordingly, genetic mutations that alter Hh signaling are associated with a wide range of birth defects and cancers, some of which are being treated with drugs that inhibit Hh signaling (Anderson *et al.* 2012; Petrova and Joyner 2014; Pak and Segal 2016). In *Drosophila* and in mammals, cells respond to Hh primarily by altering the activity of Gli-family transcription factors (Hui and Angers 2011; Xiong *et al.* 2015; Pak and Segal 2016). In the absence of Hh, the primary translation products of *Drosophila* Cubitus interruptus (Ci), as well as mammalian Gli-2 and Gli-3 orthologs, are proteolytically processed to C-terminally truncated forms that readily enter the nucleus and repress Hh target genes, while unprocessed full-length proteins remain largely cytoplasmic and inactive. When Hh binds to Patched (Ptc) and its coreceptors, the seven-transmembrane domain Smoothened (Smo) protein is activated with two key consequences; inhibition of Ci/Gli-2/3 processing and activation of full-length Ci/Gli transcriptional activators, including Gli-1, which is not subject to processing.

Ci/Gli processing involves phosphorylation by Protein Kinase A (PKA) and other protein kinases, scaffolded by a kinesin-like protein (Cos2/Kif7), to create a Cul1-dependent E3 ubiquitin ligase binding site; Hh is thought to inhibit Ci-155 processing by promoting dissociation of these phosphorylation complexes (Hui and Angers 2011; Xiong *et al.* 2015; Pak and Segal 2016). Inhibition of Ci-155 processing reduces or eliminates Ci-75 repressor but also increases Ci-155 levels. Ci-75 repressor maintains some key Hh target genes silent outside Hh signaling territory, but the relative importance of eliminating the repressor and increasing the levels of Ci-155 in cells responding to Hh has not been satisfactorily determined. High levels of Hh also promote Ci-155 degradation via a Cul3-dependent E3 ubiquitin ligase that has been

doi: https://doi.org/10.1534/genetics.117.202457
Manuscript received March 29, 2017; accepted for publication June 15, 2017; published Early Online June 21, 2017.
Supplemental material is available online at www.genetics.org/lookup/suppl/doi:10.1534/genetics.117.202457/-/DC1.
[1]These authors contributed equally to this work.
[2]Corresponding author: Department of Biological Sciences, Columbia University, 1013 Fairchild Bldg., 1212 Amsterdam Ave., New York, NY 10027. E-mail: ddk1@columbia.edu

considered as a possible negative feedback mechanism for limiting Ci-155 activity (Ohlmeyer and Kalderon 1998; Kent *et al.* 2006; Zhang *et al.* 2006). Altogether, the contribution of changes in Ci-155 levels to Hh signaling are complex and have been hard to assess.

The mechanism of full-length Ci/Gli activation is understood only in outline. It is thought principally to involve relief of inhibition by Suppressor of fused [Su(fu)], which binds directly to Ci/Gli proteins and, in *Drosophila*, it depends on Hh-activated Fused (Fu) protein kinase activity (Humke *et al.* 2010; Tukachinsky *et al.* 2010; Zhou and Kalderon 2011; Han *et al.* 2015; Oh *et al.* 2015; Zhang *et al.* 2016). It is also unclear to what degree regulation of Ci-155 activation, Ci-155, and Ci-75 levels must collaborate to produce graded Hh signaling. Dose-dependent signaling can be studied in wing discs by the quantitative induction of the universal Hh target gene, *ptc*, and the induction of target genes induced by low levels (*decapentaplegic*; *dpp*), intermediate levels (*collier*; *col*), or only by high levels (*engrailed*; *en*) of signaling (Vervoort 2000). There is some evidence of apparent redundancy, perhaps as a means to support robust signaling in a variety of settings. For example, Hh signaling is normal in the absence of Su(fu), suggesting that regulation of Ci-155 activation can be largely dispensable (Preat 1992; Ohlmeyer and Kalderon 1998). Conversely, synthetic activation of Fu kinase, which promotes Ci-155 activity, can suffice to induce strong Hh pathway activity without the strong inhibition of Ci-155 processing that normally accompanies Hh signaling (Zhou and Kalderon 2011).

To uncover new insights into the regulation of Ci-155 levels and activity we conducted a genetic screen in a sensitized background of diminished Hh signaling lacking any regulatory input from Fu kinase activity. Surprisingly, the screen revealed proteins involved in RNA processing, including core components of the Exon Junction Complex (EJC), which has recently been implicated in regulating RNA splicing (Roignant and Treisman 2010; Ashton-Beaucage and Therrien 2011; Hayashi *et al.* 2014; Malone *et al.* 2014; Le Hir *et al.* 2016), and the serine-arginine rich (SR) protein, Srp54. We provide evidence that the EJC and Srp54 target *ci* splicing to influence Hh signaling by altering the levels of Ci-155 primary translation product. We also explore the role of an alternative *ci* RNA and its presumed translation product.

Materials and Methods

Drosophila stocks

Drosophila stocks were maintained on standard cornmeal/molasses/agar medium at room temperature. For the modifier screen, *yw hs-flp* fu^{mH63}; *FRT42D P*[Fu^{+}, w^{+}] *P*[y^{+}]/*Cyo*; *Su*(*fu*)^{LP} *C765-GAL4 ptc-lacZ/TM6B* females were crossed to males with second or third chromosome deficiencies over balancer chromosomes from the Bloomington deletion library (Ryder *et al.* 2007) to produce male progeny lacking Fu kinase activity and heterozygous for both *Su*(*fu*) and the tested deficiency. The same females were crossed to *UAS-RNAi* (*upstream activating sequence-RNA interference*) stocks with or without *gCi* transgenes (16-kb genomic segments constructed as described in the section below) or ci^{94}/*Dp*(*1*;*4*)*1021*, y^{+}, $sv^{spa\text{-}pol}$ to examine wing discs from male *y* (*fu* mutant) larval progeny. To analyze adult *fu* mutant male progeny with straight wings, the *CyO* balancer was replaced with *Sp* in the parental females.

yw hs-flp; *Sp/Cyo*; *C765-GAL4 ptc-lacZ/TM6B* females were crossed to *UAS-RNAi* transgenes (with or without *gCi* transgenes or *UAS-Srp54* or *UAS-CG3605* transgenes) to examine wing discs of progeny with normal Fu and Su(fu) activities. *C765-GAL4* is expressed throughout developing wing discs. *UAS-RNAi* lines for *CG3605* (GD-26250) and *Srp54* (GD-51088) were recombined with *UAS-Diap1* on the third chromosome (BL-6657); second chromosome *UAS-mago RNAi* and *UAS-Y14 RNAi* were provided by J. E. Treisman (Roignant and Treisman 2010) and other RNAi lines tested were from the Bloomington *Drosophila* Stock Center or from the Vienna *Drosophila* Resource Center (prefaced by GD or KK) (Dietzl *et al.* 2007), including those for *eIF4AIII* (KK-108580) and *btz* (GD-38722).

Clones in a Minute background were made by crossing *yw hs-flp*; *FRT42D M*(*2*)*53*[*1*] *P*[*hs-GFP*, y^{+}]; *ptc-lacZ/TM6B* females to *FRT42D* $Y14^{\Delta 18}$ *dark/CyO* males from J. E. Treisman (who also provided *UAS-MAPK* stocks) (Roignant and Treisman 2010).

To generate MARCM (mosaic analysis with a repressible clone marker) clones with activated Fu (and loss of *smo* activity) with or without *UAS-RNAi* expression (*UAS-Diap1* was used as a control whenever testing *UAS-Srp54 RNAi* plus *UAS-Diap1*), *yw hs-flp UAS-GFP*; smo^{2} *FRT42D P*[smo^{+}] *tub-Gal80*; *C765 ptc-lacZ/TM6B* females were crossed to *yw*; smo^{2} *FRT42D* (*UAS-mago RNAi*) *UAS-GAP-Fu*; (*UAS-Diap1*) (*UAS-Srp54 RNAi*) males. For *smo cos2* clones and *ptc* clones, males had $cos2^{2}$ or ptc^{S2}, respectively, in place of *UAS-GAP-Fu*.

For *pka* clones, *yw hs-flp UAS-GFP*; *tub-Gal80 FRT40A*; *C765 ptc-lacZ/TM6B* females were crossed to *yw hs-flp*; *pka-*$C1^{H2}$ *FRT40A* (*UAS-mago RNAi*)*/Cyo*; (*UAS-Diap1*) (*UAS-Srp54 RNAi*) males. In all cases, clones were induced by a 1-hr heat-shock at 37° of first and second instar larvae.

To test replacement of *ci* with *gCi* or *UAS-Ci* transgenes in MARCM clones, *yw hs-flp UAS-GFP*; *FRT42D P*[ci^{+}, w^{+}] *tub-GAL80/CyO*; *C765-GAL4 ptc-lacZ/TM6B*; ci^{94}/*Dp*(*1*;*4*)*1021*, y^{+}, $sv^{spa\text{-}pol}$ females were crossed to *yw*; *FRT42D*; *gCi or UAS-Ci*; ci^{94}/*Dp*(*1*;*4*)*1021*, y^{+}, $sv^{spa\text{-}pol}$ males.

To test rescue of ci^{94} null animals, *ptc-lacZ*; ci^{94}/*Dp*(*1*;*4*)*1021*, y^{+}, $sv^{spa\text{-}pol}$ females were crossed to *gCi* (or derivatives); ci^{94}/*Dp*(*1*;*4*)*1021*, y^{+}, $sv^{spa\text{-}pol}$ males. Rescue in the presence of ci^{Ce-2} was tested using males with this allele replacing ci^{94}.

To test RNAi effects in the presence of only *gCi* or *SV-1* in whole discs, *yw hs-flp*; *Sp/Cyo* ; *(gCi) (SV-1) C765 ptc-lacZ/TM6B*; ci^{94}/*Dp(1;4)1021*, y^{+}, $sv^{spa\text{-}pol}$ females were crossed to *yw hs-flp*: (*UAS-mago RNAi*) (*Sp*)/*Cyo*; (*gCi*) (*SV-1*) (*UAS-Srp54 RNAi*) (*UAS-Diap1*); ci^{94}/*Dp(1;4)1021*, y^{+}, $sv^{spa\text{-}pol}$

males. For the analogous test in *pka* mutant MARCM clones, *yw hs-flp UAS-GFP*; *tub-Gal80 FRT40A*; (*gCi* or *SV-1*) *C765 ptc-lacZ/TM6B*; $ci^{94}/Dp(1;4)1021, y^+, sv^{spa\text{-}pol}$ females were crossed to *yw hs-flp*; $pka\text{-}C1^{H2}$ *FRT40A/CyO*; (*gCi* or *SV-1*) *UAS-Diap1* (*UAS-Srp54 RNAi*); $ci^{94}/Dp(1;4)1021, y^+, sv^{spa\text{-}pol}$ males and *yw hs-flp UAS-GFP*; *tub-Gal80 FRT40A*; $Su(fu)^{LP}$ *C765 ptc-lacZ/TM6B*; $ci^{94}/Dp(1;4)1021, y^+, sv^{spa\text{-}pol}$ females were crossed to *yw hs-flp*; $pka\text{-}C1^{H2}$ *FRT40A UAS-mago RNAi/CyO*; (*gCi* or *SV-1*); $ci^{94}/Dp(1;4)1021, y^+, sv^{spa\text{-}pol}$ males.

All wings or stained wing discs shown were from male animals when mutant for *fu*; in all other cases, wing discs were dissected from larvae without sorting males from females.

Mutagenesis and cloning

Genomic transgenes were created by cloning the entire 16-kb genomic *ci* region from a Bluescript-SK (BSK) vector [provided by K. Basler (Methot and Basler 1999)] into an att-Pacman Expression vector (*Drosophila* Genomics Resource Center). To facilitate mutagenesis, the 16-kb fragment was first separated into two parts. The region including the promoter, first exon, and part of the first intron ("Ci fragment 2") was cloned as a *Bam*HI-*Nhe*I fragment into BSK cut with *Bam*HI and *Xba*I to create BSK-CiF2. The complementary *Nhe*I-*Kpn*I fragment containing all other exons and the 3′-UTR ("Ci Fragment 1") was cloned into BSK cut with *Spe*I and *Kpn*I to create BSK-CiF1. BSK-CiF2 was cut with *Not*I and *Bsp*1201 to clone the whole CiF2 fragment into the P[acman]-Cm^R vector cut with *Not*I, so that *Rsr*II and *Pme*I vector sites were downstream of *ci* first intron sequences in RP-CiF2. CiF1 was amplified from BSK-CiF1 by long-range PCR using PfuUltraII Fusion HS DNA polymerase (Agilent Technologies), adding *Rsr*II and *Pme*I at either end and cloning the product into a Zero Blunt Topo cloning vector (Invitrogen, Carlsbad, CA). The *Rsr*II-*Pme*I fragment was then cloned into RP-CiF2 cut with the same enzyme to create the final Pacman vector containing the entire 16 kb genomic ci DNA. The 28 kb gCi AttPacman transgene was then inserted at the *att ZH-86Fb* landing site at cytological location 86F8 (Rainbow Transgenic Services). To create *gCi ATG-A* and *gCi ATG-B*, ATG codons were first altered in BSK-CiF2 and BSK-CiF2, respectively, using the QuikChange II site-directed mutagenesis kit (Agilent Technologies) (primers are listed in Supplemental Material, Table S2 in File S1). To create *SV-1* and *Ci-1*, Ci coding sequences were amplified from a full-length *ci* cDNA using primers beginning 2- nt upstream of the initiation codon and at the stop codon but preceded by an added *Xba*I site. This amplicon was partially digested with *Aat*II and *Xba*I to generate a 4.2-kb coding region fragment that was cloned between *Aat*II (which cuts 23 nt upstream of the initiation codon for Ci-A) and *Xba*I sites of BSK-CiF2. The resulting DNA was cut with *Bsp*1201 and *Not*I to release an 11.5-kb fragment that was cloned into the *Not*I site of attB-P[acman]-Ap^R (producing att-BP[acman]-PCi). A 1-kb segment of DNA downstream of the stop codon was amplified by PCR from BSK-CiF1, adding *Not*I and *Pac*I to either end, and cloned between the *Not*I site and *Pac*1 sites of att-BP[acman]-PCi to produce the *Ci-1* transgene. Alternatively, the 3′-UTR from SV40 was amplified from pUAST-attB with addition of *Not*I and *Pac*I sites and cloned similarly into att-BP[acman]-PCi to produce the *SV-1* transgene. The *UAS-Srp54* transgene was constructed by amplifying the coding region from the FBcI0164286 cDNA clone (DGRC) with addition of *Not*I and *Xho*I sites, followed by cloning into pUAST-attB and introduction into the 86F *att* landing site. An analogous method was used to make *UAS-CG3605*, starting from the FBcl10177075 cDNA clone (DGRC), adding *Eco*RI and *Kpn*I sites to clone it into *pUAST-attB*.

Immunohistochemistry

Wing discs were dissected from late third instar larvae in PBS and fixed in 4% paraformaldehyde (in PBS) for 30 min, rinsed 3× with PBS, blocked with 10% normal goat serum (Jackson ImmunoResearch Laboratories) in PBST (0.1% Triton) for 1 hr, and stained with the following primary antibodies: rabbit anti-caspase 3 (1:100; D175, Cell Signaling), rabbit anti-β-galactosidase (1:10000; MP Biomedicals), mouse 4D9 anti-engrailed (1:5; Developmental Studies Hybridoma Bank), rat 2A1 anti-Ci (1:3; Developmental Studies Hybridoma Bank), and mouse anti-collier (1:10,000 from Alain Vincent, Toulouse University, France) overnight at 4°. Inverted larvae were then washed three times in PBST for 10 min each and incubated with Alexa Fluor 488, 546, 594, or 647 secondary antibodies (1:1000; Molecular Probes, Eugene, OR) for 1 hr at room temperature. Larvae were washed twice in PBST for 20 min each, once in PBS for 10 min, and mounted, with or without additional Hoechst staining (1:1000; Molecular Probes), in Aqua/Poly mount (Polysciences, Warrington, PA).

Quantitation from fluorescent images

Fluorescence images were captured using 20×, or 63×, 1.4 NA oil immersion lenses on a confocal microscope (LSM 700; Zeiss [Carl Zeiss], Thornwood, NY). Whole wing disc images of 512 × 512 pixels at 8-bit depth were captured with a 20× lens at a resolution of 2.52 pixels/μm. Three stacks per wing disc where acquired with xzy scaling of 645, 645, and 5.3 μm. Centering of the middle stack was done based on the highest levels of *ptc-lacZ* and Ci-155 at the dorsal/ventral (D/V) boundary. The range indicator was used to set the appropriate laser intensity per experiment for each fluorophore such that the signal was in the linear range. Rotation and *z*-projection of the stacks were performed with ImageJ software (National Institutes of Health, Bethesda, MD). To measure intensity profiles along the anterior/posterior (AP) axis, an elongated rectangle was drawn on a central region of the wing pouch, avoiding the DV border. The *y*-axis shows the average fluorescence intensity over the height of the rectangle at each point on the *x*-axis (AP axis) for *ptc-lacZ* expression or Ci-155 protein, measured using Image J. At least three wings discs per condition were measured and averaged for each plot, using the posterior edge of *ptc-lacZ* expression as a reference point for the AP border. The ratio of the peak fluorescence intensity at the AP border for an experimental genotype relative to the

appropriate control processed in parallel was calculated for each experiment. These values (expressed as a percentage of controls) from at least three independent experiments were used to calculate a mean and C.I. For clones, the average fluorescent intensity over the area of the GFP-marked clone was measured using Image J. The average fluorescence intensity in anterior cells outside the clones in the same wing disc was also measured. From these measurements, the ratio of fluorescence intensities (inside/outside) was calculated for each clone. These values from multiple control and experimental clones were used to derive mean and SEM values. Representative images of clones were acquired with a 63×, 1.4 NA oil immersion lens at a resolution of 2.52 pixels/μm.

Adult wings

Adult wings were pulled off anesthetized flies and placed in 70% ethanol for 5 min, transferred to 100% ethanol, and then mounted in Aqua/Poly Mount (Polysciences). They were imaged with Transmitted Light on a Nikon Diaphot 300 microscope at 10× (Nikon, Garden City, NY).

RNA analysis

For analysis, 30–40 wing discs per genotype were dissected from third instar larvae in cold nuclease-free PBS. RNA was isolated from the wing discs using an RNeasy mini kit (QIAGEN, Valencia, CA) with DNase (QIAGEN) and converted to cDNA using the Maxima H Minus First Strand cDNA Synthesis Kit (Thermo Scientific) using random primers or oligodT. Quantitative RT-PCR was performed in the StepOnePlus Real-Time PCR System with Power SYBR Green Mastermix (Applied Biosystems, Foster City, CA). Primers for amplifying each PCR product are listed in Table S3 in File S1. The relative abundance of RNAs for experimental discs *vs.* controls was calculated using the $2^{-\Delta\Delta Ct}$ method, normalizing to the housekeeping genes Rpl15 and α4-tubulin. The level of *ci-B* RNA relative to *ci-A* RNA was calculated from the Ct values for each.

Statistics

To compare experimental values to controls for fluorescence intensity (of *ptc-lacZ* expression or Ci-155 protein) measured at the AP border of wing discs, the experimental/control ratio was first calculated from individual trials using at least three wing discs of each genotype, as described earlier. These ratios from multiple trials were then used to calculate a mean value and 95% C.I. for each experimental genotype, expressed as a percentage of control values. Mean values and C.I.s of experimental samples expressed as a percentage of controls were calculated analogously for RNA measurements after converting raw quantitative (q)RT-PCR results into an experimental/control ratio for each trial. For measurements of fluorescent intensity in clones, the average clone intensity relative to surrounding anterior cells was first calculated for experimental and control samples, as described earlier. The set of values obtained from multiple clones of each genotype were examined by a Shapiro–Wilk test for a fit to a normal distribution. Mean values for experimental and control clones were then calculated and a *P*-value for the significance of differences between them was calculated using an unpaired Student's *t*-test for unequal variances. For each experiment, the number of samples and trials are given in the figure legend. The number of samples or trials was not predetermined; we aimed to test as many samples as possible (some required genotypes were rare among progeny). No samples were excluded for reasons other than poor staining or physical damage during processing.

Data availability

The authors state that all data necessary for confirming the conclusions presented in the article are represented fully in the article. *Drosophila* stocks and other reagents are available upon request.

Results

EJC and splicing factors identified in a screen for modifiers of Hh pathway activity

Hh is expressed in posterior compartment cells of the wing disc and is transported to a strip of neighboring anterior cells to induce transcription of several patterning genes at the AP border (Vervoort 2000; Xiong *et al.* 2015). These Hh target genes include *ptc*, conveniently reported by the level of *ptc-lacZ* expression, and *col* (Figure 1, G and H), which is essential for specifying the tissue between the central two veins of the mature wing. To identify new contributors to Hh signaling pathway activity, we tested a large set of heterozygous autosomal deficiencies for the ability to modify the wing phenotypes of flies heterozygous for *Su(fu)* and lacking Fu kinase activity; these flies have reduced intervein territory between veins 3 and 4 (v3–4, Figure 1, A and B) resulting from impaired Hh signaling. Only two deficiencies, including *Su(fu)* and *cos2*, respectively, increased v3–4 separation, consistent with enhanced Hh pathway activity (Table S1 in File S1). For each deficiency that narrowed the v3–4 interval, we tested several additional deletions to define a critical region. Ten intervals with at least two overlapping deficiencies narrowing v3–4 were identified from a total of ~220 deficiencies successfully screened (Table S1 in File S1).

The phenotype of one deficiency was reproduced by a point mutation in the *tsunagi* (*tsu*; aka *Y14*) gene (Figure 1C). Because Y14 and Mago nashi (Mago) are core members of the EJC, we also tested a null mutation of *mago* as a modifier and found that it also narrowed v3–4 spacing (Figure 1D). This spacing could theoretically be altered by reducing Hh pathway activity or by affecting downstream steps. The latter mechanism is likely for a set of overlapping deficiencies that included *spalt* and *spalt-related*, which have established roles in vein specification (Organista *et al.* 2015) (Table S1 in File S1). The MAPK *rolled* is also involved in vein formation and is a known target of Mago and Y14 (Blair 2007; Ashton-Beaucage *et al.* 2010; Roignant and Treisman 2010). However, the *mago* phenotype was not reversed by ectopic expression of a *UAS-MAPK* transgene shown previously to rescue MAPK

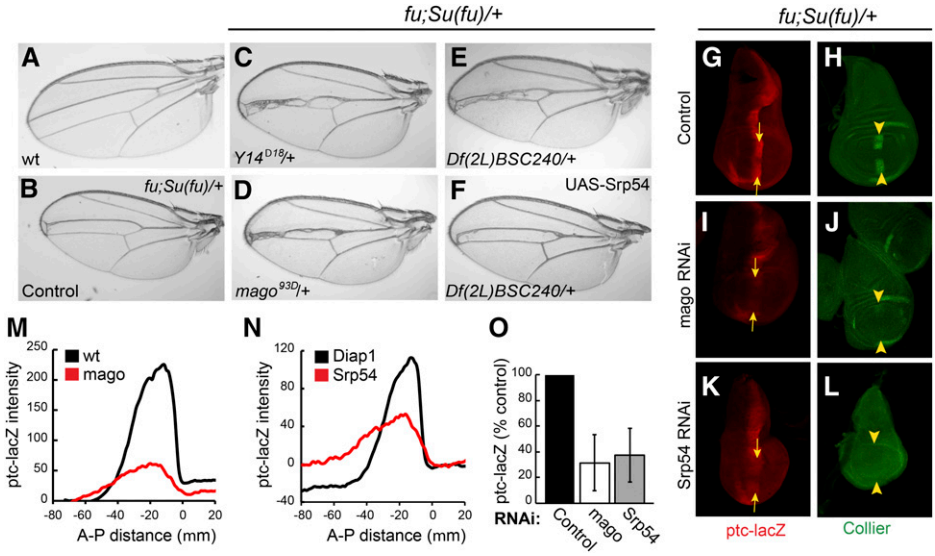

Figure 1 Screen for Hh pathway modifiers. (A–F) Wings from (A) wild-type males and (B–F) *fu*; *Su(fu)*/+ males. (B) Narrowing of the central veins was increased by heterozygosity for (C) $Y14^{\Delta 18}$ and (D) $mago^{93D}$. Narrowing due to (E) *Df(2L) BSC240* was (F) largely suppressed by expression of *UAS-Srp54* cDNA with *C765-GAL4*. (G and H) Wing discs from *fu*; *Su(fu)*/+ larvae have reduced expression at the AP border (yellow arrows) of (G) *ptc-lacZ* (red) and (H) Collier [green; restricted to the wing pouch (arrowheads)] relative to wild-type (data not shown). (I–L) Both *ptc-lacZ* and Collier were reduced further by *C765-GAL4*-driven expression of (I and J) *UAS-mago RNAi* or (K and L) *UAS-Srp54 RNAi* together with *UAS-Diap1* (*UAS-Diap1* was always used as a control for this genotype). Reduced *ptc* induction limits Ptc-induced endocytosis of Hh, so a weaker *ptc-lacZ* AP border stripe is also generally broader. (M and N) Average *ptc-lacZ* intensity along the AP axis (anterior to the left of zero) of the wing pouch for four wing discs in a single experiment, comparing (M) *UAS-mago RNAi* to control and (N) *UAS-Srp54 RNAi* to control (both also express *UAS-Diap1*). (O) Maximal *ptc-lacZ* intensity at the AP border (derived from profiles along the AP axis) as a percentage of controls for discs expressing *mago* and *Srp54* RNAi, showing means and 95% C.I.s ($n = 4$ experiments for *mago RNAi* and $n = 3$ experiments for *Srp54 RNAi*). AP, anterior/posterior; Hh, Hedgehog; Ptc, Patched; RNAi, RNA interference; wt, wild-type.

function impaired by EJC depletion (Roignant and Treisman 2010) (Figure S1, D and E in File S1). Thus, Mago is not acting via MAPK and may instead be affecting the Hh pathway.

To identify the key gene within two additional narrowly defined deletion intervals, we tested the consequence of expressing all relevant available *UAS-RNAi* transgenes in a sensitized (*fu*; *Su(fu)*/+) background using *C765-GAL4*, which is expressed selectively in wing discs. RNAi directed toward the genes *CG4602* (*Srp54*) and *CG3605* did not permit eclosion of any adults but significantly reduced the activity of the universal Hh pathway reporter, *ptc-lacZ*, at the AP border of third instar larval wing discs (Figure S2C in File S1 and data not shown). However, both also variably reduced the size of wing discs, disrupted nuclear integrity, and induced activated caspase 3 staining, indicative of apoptosis (Figure S2C' in File S1 and data not shown). Coexpression of the antiapoptotic *Diap1* gene largely rescued these phenotypes for *Srp54 RNAi* (Figure S2, A'–D' in File S1) but less completely for RNAi toward *CG3605*. In both cases, there was still a marked reduction in *ptc-lacZ* staining at the AP border of wild-type or *fu*; *Su(fu)*/+ wing discs (Figure 1, G, K, N, and O and Figures S1, F–M and S2, A–D in File S1). Expression of *UAS-Srp54* using *C765-GAL4* largely reversed the v3–4 narrowing of *fu*; *Su(fu)*/+ flies due to *Df(2L) BSC240* (Figure 1, E and F), while *UAS-CG3605* partially suppressed v3–4 narrowing due to *Df(2L) Exel7014* (Figure S1, A–C in File S1), suggesting that *Srp54* and *CG3605* were critical modifier genes within the two deficiencies that affected Hh pathway activity. Srp54 belongs to the family of SR proteins, which contain RNA-binding and Arg/Ser-rich domains, and are generally involved in RNA splicing (Bradley *et al.* 2015). Both Srp54 and *CG3605* have been identified in spliceosomal complexes and functionally implicated in RNA splicing (Kennedy *et al.* 1998; Park *et al.* 2004; Wu *et al.* 2006; Herold *et al.* 2009).

Collier is induced at the AP border of wing discs by moderately high levels of Hh signaling (Vervoort 2000) and consequently has lower expression in a *fu*; *Su(fu)*/+ background than in wild-type wing discs. Expression of Collier was eliminated by additional expression of *Srp54* or *CG3605 RNAi* transgenes (Figure 1, H, J, and L and Figure S1, F' and H' in File S1). Likewise, *mago RNAi* eliminated Collier induction at the AP border of *fu*; *Su(fu)*/+ wing discs and strongly reduced *ptc-lacZ* expression (Figure 1, G–J, M, and O), directly implicating Mago in Hh signaling. Expression of *mago RNAi* did not induce cell death or other morphological phenotypes. Because the apoptotic phenotype of *CG3605* inhibition was not fully suppressed by Diap1, we focused further studies on just Srp54 and Mago, and always expressed excess Diap1 together with *Srp54 RNAi* to suppress cell death.

Mago and Srp54 alter Ci-155 levels

The effects of reducing Mago and Srp54 activity on Hh pathway activity and the levels of Ci-155 were measured in otherwise wild-type wing discs. Mago inhibition lowered Ci-155 levels at the AP border and in anterior regions by ~30% (Figure 2, G, H, K, and M). RNAi transgenes directed to two other core pre-EJC components, Y14 and eIF4AIII, also reduced Ci-155 levels in wild-type wing discs and reduced *ptc-lacZ* expression in wing discs with impaired Hh signaling (*fu*; *Su(fu)*/+) (Figure S3 in File S1). Hh pathway activity, measured by expression of *ptc-lacZ* and the high-level Hh target gene, Engrailed (En) at the AP border, was not inhibited by RNAi directed to Mago, Y14, or eIF4AIII in wild-type wing discs (Figure 2, A, B, D, and F and data not shown). Inhibition of Barentsz (Btz), which is a largely cytoplasmic core EJC component (MLN51 in mammals), did

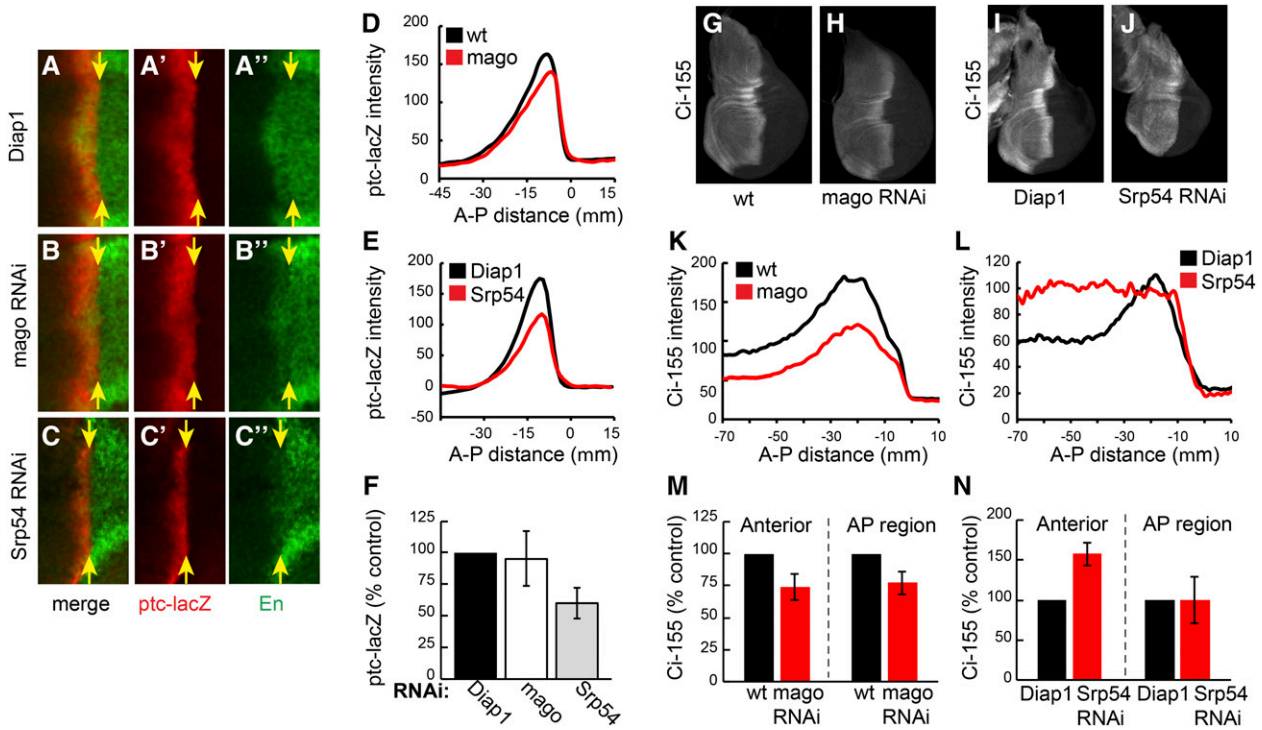

Figure 2 Different effects of Mago and Srp54 inhibition on Ci-155 levels and activity. (A–C) Central region (around DV and AP borders) of wing discs expressing (A) *UAS-Diap1*, (B) *UAS-mago RNAi*, and (C) *UAS-Srp54 RNAi* plus *UAS-Diap1* under the control of *C765-GAL4*, stained for *ptc-lacZ* (red) and Engrailed (En; green). Only Srp54 RNAi reduced *ptc-lacZ* expression and prevented Hh induction of anterior En (to the left of yellow arrows indicating the posterior edge of the AP border). (D and E) *ptc-lacZ* intensity profiles along the AP axis for (D) *UAS-mago RNAi* and (E) *UAS-Srp54 RNAi* compared to controls for a single experiment (average of 3–4 discs). (F) Maximal *ptc-lacZ* intensity as a percentage of controls for discs expressing *mago* and *Srp54 RNAi*, showing means and 95% C.I.s (n = 6 experiments for *mago RNAi* and n = 3 experiments for *Srp54 RNAi*). (G–J) Wing discs expressing (H) *UAS-mago RNAi*, (J) *UAS-Srp54 RNAi*, and (G and I) controls, stained for Ci-155 (white). (K–L) Ci-155 intensity profiles along the AP axis for single experiments (average of four wing discs), comparing (K) Mago and (L) Srp54 inhibition to controls. (M and N) Maximum Ci-155 intensity in anterior and AP border cells as a percentage of controls for discs expressing *mago* and *Srp54* RNAi, showing means and 95% C.I.s (n = 5 experiments for *mago RNAi* and n = 4 experiments for *Srp54 RNAi*). AP, anterior/posterior; DV, ; Hh, Hedgehog; Ptc, Patched; RNAi, RNA interference; wt, wild-type.

not alter *ptc-lacZ* expression in *fu*, *Su(fu)/+* wing discs or Ci-155 levels (Figure S3, D, E, J, and K). A nuclear function of Mago, Y14, and eIF4AIII that is not shared by Btz has been demonstrated for normal splicing of *MAPK* and *piwi* in *Drosophila* (Roignant and Treisman 2010; Ashton-Beaucage and Therrien 2011; Hayashi *et al.* 2014; Malone *et al.* 2014). Therefore, we hypothesized that Mago, Y14, and eIF4AIII core EJC components affect Hh pathway activity under sensitized conditions by acting directly on *ci* RNA splicing to reduce Ci-155 protein levels.

Reduction of Srp54 activity also altered the profile of Ci-155 in wing discs but in a different manner. Ci-155 levels were not significantly altered at the AP border but were higher throughout the rest of the anterior compartment compared to wild-type discs (Figure 2, I, J, L, and N). Inhibition of Srp54 also reduced *ptc-lacZ* expression and almost eliminated anterior En expression at the AP border of wild-type wing discs (Figure 2, A, C, E, and F). The changes in Ci-155 levels and *ptc-lacZ* expression due to *Srp54 RNAi* were suppressed by expression of an *Srp54* cDNA (Figure S2, E–H), confirming attribution to Srp54. The observed Ci-155 profile suggests that *Srp54 RNAi* may impair Ci-155 processing in anterior cells, so that Ci-155 levels cannot reliably report any additional changes in *ci* RNA.

Effects of Mago and Srp54 inhibition on ci RNA

The most direct way that Mago might alter Ci-155 levels is by acting on *ci* RNA. The major documented *ci* RNA is denoted *ci-A* but a much less prevalent RNA, *ci-B*, has been deduced from a small number of cDNAs and RNA-seq data (FlyBase). Those data suggest that *ci-B* RNA initiates at a site upstream of *ci-A* and uses an alternative splice donor at the end of the first exon that is just 8 nt downstream of the *ci-A* 5′-end (Figure 3A). Using RNA from wild-type wing discs we were able to detect a product of the expected size using primers corresponding to exon 1B and exon 2, but at much lower levels than for an exon 1A to exon 2 primer pair (Figure 3B). These data confirm the presence of *ci-B* RNA in wing discs. The absence of a larger product corresponding to the E1A splice donor when using primer 1B supported the idea that RNAs initiating upstream of the E1B primer use only the E1B donor splice site. qRT-PCR experiments with the same primer pairs indicated that *ci-A* is roughly 200-fold more abundant than *ci-B* in wing discs (difference between Ct values was 7.5 ± 0.64).

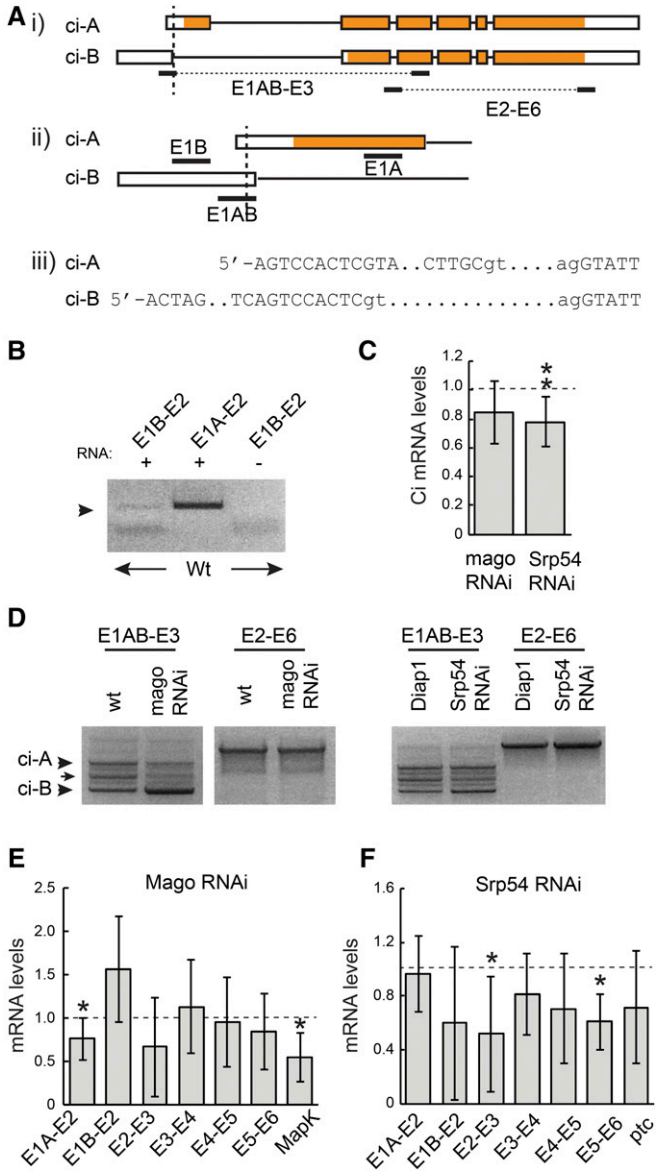

Figure 3 Mago and Srp54 regulate *ci* RNA. (A) Schematic representation of *ci-A* and *ci-B* RNAs, together with primer locations (exons are boxed with translated segments in orange). The TSS of B is 742 nt upstream of TSS-A. *ci-B* first exon donor splice site is 8 nt downstream of TSS-A. *ci-A* first exon is 469 nt and first intron is 3446 nt; *ci-B* first exon is 751 nt and first intron is 3906 nt. (B) RT-PCR products from wild-type wing disc RNA using the indicated primer pairs. (C) *ci* RNA levels as a fraction of controls (set at 1.0; dashed line) measured by qRT-PCR with primers from exon 3 and spanning the exon 2/3 junction for total RNA from wing discs expressing *mago RNAi* or *Srp54 RNAi*. (D) RT-PCR products obtained using the indicated primer pairs using RNA from wing discs with reduced Mago, Srp54, or their controls. Products of the expected sizes for *ci-A* and *ci-B* (arrowheads) were confirmed by sequencing. An intermediate band (arrow) revealed a clear product on one occasion, corresponding to splicing between the *ci-B* donor site and an acceptor 277 nt downstream, followed by splicing in the *ci-A* pattern (and therefore encoding the normal Ci-A protein product). (E and F) RNA levels as a fraction of controls (set at 1.0; dashed line) measured by qRT-PCR using primers spanning each exon junction of *ci* and exons 6–7 of MAPK for wing discs expressing (E) *UAS-mago RNAi* or (F) *UAS-Srp54 RNAi* compared to controls. (C, E, and F) Values in all qRT-PCR experiments were first normalized to Rp49 and Rpl45 levels. Means and 95% C.I.s are shown relative to controls (set at 1.0) for (C) $n = 9$ experiments and (E and F) $n = 3$ experiments for all except E1A–E2 for *mago* and *Srp54 RNAi* ($n = 7$), E1B–E2, E2–E3, E4–E5, and E5–E6 for *mago RNAi* ($n = 4$), MAPK ($n = 5$), and E5–E6 for *Srp54 RNAi* ($n = 4$). Significant differences to controls were also calculated by Student's *t*-test (* $P < 0.05$, ** $P < 0.01$). qRT-PCR, quantitative RT-PCR; RNAi, RNA interference; TSS, transcription start site; wt, wild-type.

We then explored whether inhibition of Mago or Srp54 altered the amounts or splicing patterns of these *ci* RNAs.

We observed reduced levels of *ci* RNA by qRT-PCR using primers that amplified sequences in exon 3 for both *mago* and *Srp54 RNAi* treatments of wing discs (Figure 3C). To compare *ci-A* and *ci-B* RNA levels, while selectively increasing detection sensitivity for *ci-B* RNA we used a primer (E1AB) that matched exon 1B throughout its 20 nt but matched exon 1A only at the last 9 nt. Using this primer together with an exon 3 primer for RT-PCR revealed three clear bands (Figure 3D). Two were sequenced and found to correspond to the expected sequences of *ci-A* and *ci-B* in this region. The ratio of these two bands was not discernibly altered in wing discs expressing *Srp54 RNAi* but Mago inhibition significantly increased the *ci-B* product relative to *ci-A* (Figure 3D). No novel RNA splicing patterns or included introns were detected in response to Mago or Srp54 inhibition for regions spanning exons 1–3 or 2–6 (Figure 3D). qRT-PCR measurements supported the inference that RNA with the splice characteristic of *ci-B* was increased, while RNA with the *ci-A* splice was reduced in response to Mago inhibition (Figure 3E).

RNA spliced across introns common to *ci-A* and *ci-B* was reduced by *mago RNAi* in some cases, but not consistently (Figure 3E). A known Mago target in the *MAPK* gene was used as a positive control (Roignant and Treisman 2010) and showed reduced spliced product, as expected. The alteration in the pattern of *ci* RNAs suggests that Mago may act directly on *ci* splicing. Loss of Mago may be affecting the choice of splice donor sites for the first exon to allow some E1B donor use for the major *ci* primary transcript. Alternatively, loss of Mago might be affecting the choice of transcription start sites, increasing initiation at the upstream site characteristic of *ci-B* and decreasing initiation from the major *ci-A* start site. In either case, the reduced levels of E1A–2 spliced RNA observed (Figure 3, D and E) would be expected to decrease Ci-155 protein levels, while increased *ci-B* RNA levels would only produce a very small increase in protein product because this RNA is present at only ~1% of *ci-A* RNA levels.

Inhibition of Srp54 led to a reduction in spliced RNA across all main-body introns but, in contrast to Mago inhibition, it did not increase E1B–E2 spliced RNA or significantly reduce E1A–E2 spliced RNA levels (Figure 3, D and F). *ptc* RNA levels were reduced (Figure 3F), consistent with reduced *ptc-lacZ* expression at the AP border. The reduced amount of *ci* RNA measured across all constitutive splice junctions would be expected to result in reduced levels of Ci-155 primary translation product.

Cell autonomy of Mago and Srp54 effects on Hh pathway activity

If EJC proteins or Srp54 affect Hh signaling by acting on *ci* RNA, we would expect them to act in cells responding to Hh,

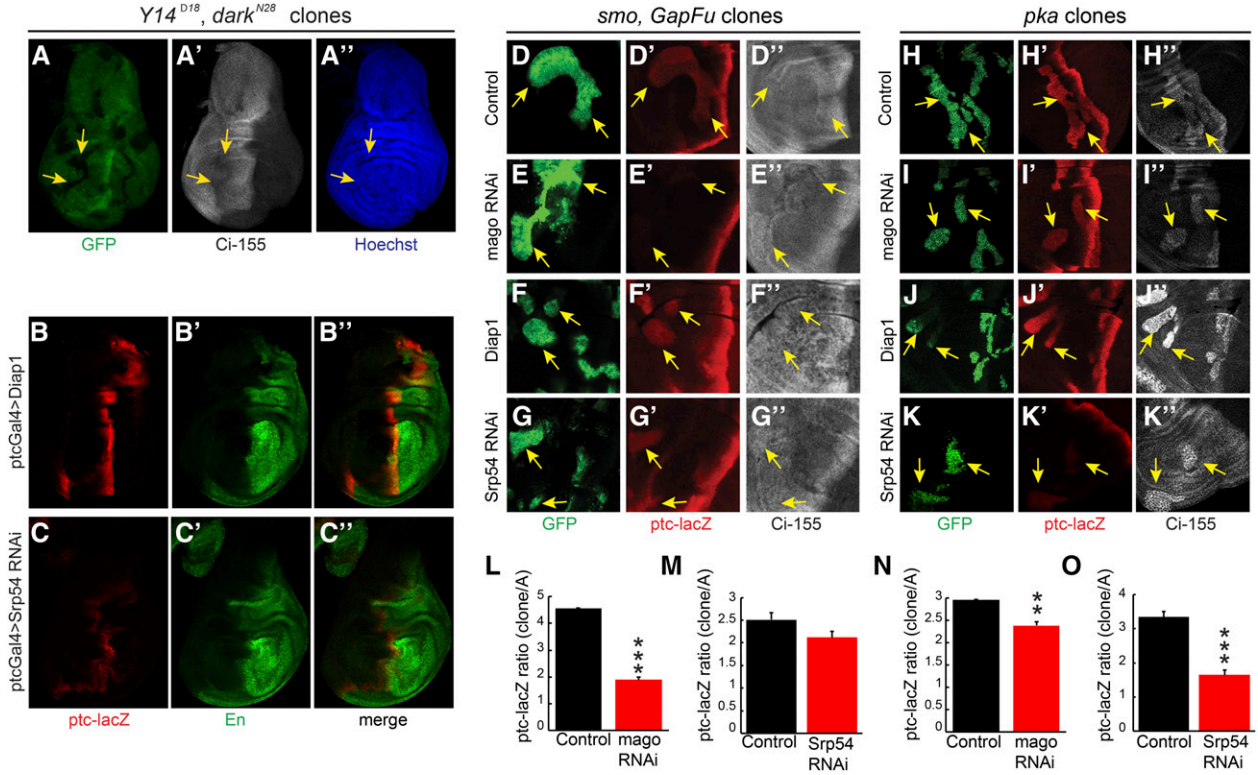

Figure 4 Cell autonomous action of EJC members and Srp54 on Hh pathway activity. (A) Homozygous $Y14^{\Delta 28}$ $dark^{N28}$ clones (arrows) in a *Minute* background, marked by loss of GFP (green), had lower Ci-155 levels [white, (A′)] but no cell death or rearrangement evident from nuclear Hoechst staining [blue, (A″)]. (B–C) Expression of *UAS-Srp54 RNAi* with *ptc-GAL4* driver reduced *ptc-lacZ* (red) and anterior En (green) expression relative to *UAS-Diap1* controls. (D–G) Ectopic *ptc-lacZ* (red) was induced in anterior *smo* clones expressing *UAS-GapFu* (marked by GFP, green, arrows) but induction was reduced (E) greatly by *UAS-mago RNAi* and (G) slightly by *UAS-Srp54 RNAi*. (D″–G″) Changes in Ci-155 levels (white) were small. (H–K) Ectopic *ptc-lacZ* (red) was induced in anterior *pka* clones (marked by GFP, green, arrows) but induction was reduced (I) slightly by *UAS-mago RNAi* and (K) greatly by *UAS-Srp54 RNAi*. (H″–K″) The increase of Ci-155 (white) was clearly reduced by Srp54 RNAi in some *pka* clones. (L–O) *ptc-lacZ* intensity relative to controls within (L and M) *smo GapFu* clones or (N and O) *pka* clones, showing mean, SEM, and significant differences calculated by Student's *t*-test (** $P < 0.001$, *** $P < 0.0001$), using (L) $n = 4$ control and $n = 8$ experimental clones, (M) $n = 13$ control and $n = 21$ experimental clones, (N) $n = 21$ control and $n = 18$ experimental clones, and (O) $n = 15$ control and $n = 16$ experimental clones. EJC, exon junction complex; En, engrailed; Hh, Hedgehog; Ptc, Patched; RNAi, RNA interference; wt, wild-type.

rather than in cells responsible for producing or transporting Hh. Strong alleles of *Y14* or *mago* did not readily produced large homozygous mutant wing disc clones but we did observe a cell autonomous reduction of Ci-155 levels for *Y14* clones when clone survival was enhanced by using a *Minute* background (Amoyel and Bach 2014) and a mutant allele of the proapoptotic *dark* gene (Roignant and Treisman 2010) (Figure 4A). We also observed a reduction in AP border *ptc-lacZ* and En expression when *Srp54 RNAi* expression was limited to anterior cells by using *ptc-GAL4* as a driver (Figure 4, B and C). However, the most convincing evidence of Mago and Srp54 acting in Hh signal transduction was observed by creating MARCM clones (Lee and Luo 2001) that expressed the corresponding *RNAi* in anterior cells and had ectopic Hh pathway activity due to genetic alteration of PKA or Fu activity.

Reduced *ptc-lacZ* expression due to *mago RNAi* was clearest in clones expressing activated Fu elicited by expression of GAP-Fu, a membrane-tethered Fu fusion protein containing the myristoylation domain from Growth-Associated-Protein-43 (Claret *et al.* 2007; Zhou and Kalderon 2011) (reduced 60%, Figure 4, D, E, and L). Reduced *ptc-lacZ* expression was also evident in *pka* (Figure 4, H, I, and N) and *cos2* (Figure S4, G, H, and K in File S1) mutant clones (reduced 20% in each case). A cell autonomous reduction of *ptc-lacZ* expression due to Srp54 inhibition was also seen for the same three types of clone. The effects of Srp54 inhibition were larger for *pka* mutant clones (reduced 50%, Figure 4, J, K, and O) than for *cos2* mutant clones (reduced ~20%, Figure S4, I, J, and L in File S1) or for clones with activated Fu (reduced 15%, Figure 4, F, G, and M). No significant reduction of *ptc-lacZ* due to Mago or Srp54 inhibition was observed in *ptc* mutant clones (Figure S4, A–F in File S1), which have very high levels of Hh pathway activity. These results are consistent with cell autonomous actions of Mago and Srp54, which contribute significantly to Hh pathway activity when the pathway is not maximally activated (as in *pka*, *cos2*, and *GAP-Fu* mutant clones and at the AP border of discs lacking Fu kinase activity).

We also observed that Ci-155 levels were reduced by *Srp54 RNAi* in *pka* mutant clones (Figure 4, J″ and K″). There is no

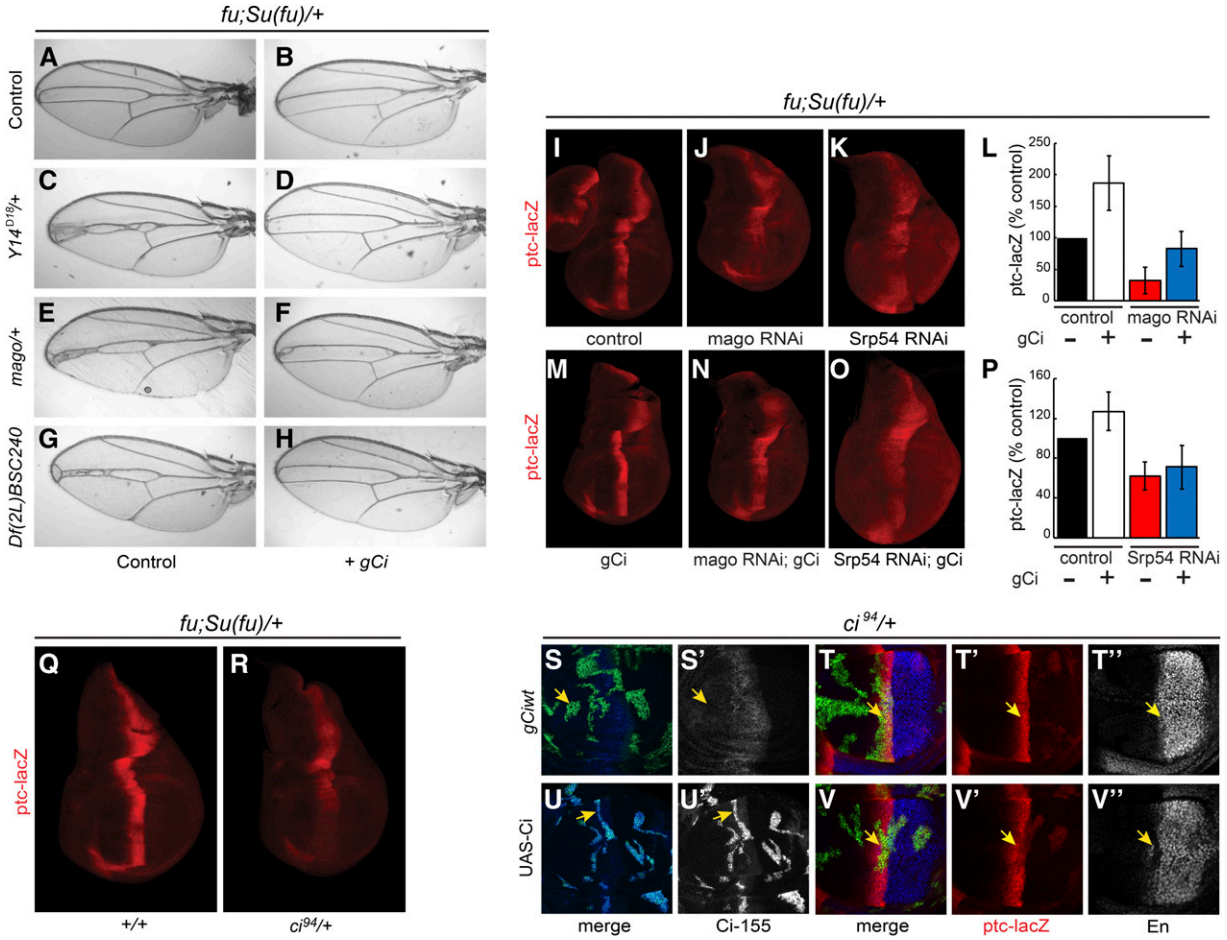

Figure 5 Dependence of Hh signaling on Ci-155 levels. (A–H) Narrowing of veins 3–4 in (A) *fu*; *Su(fu)*/+ controls is increased by heterozygosity for (C) *Y14*, (E) *mago*, or (G) *Df(2L)BSC240*, but these changes were (B, D, F, and H) suppressed by addition of a single copy of the *gCi* transgene. (I–P) In *fu*; *Su(fu)*/+ wing discs a single copy of the *gCi* transgene (I and M) increased *ptc-lacZ* expression and (J–O) suppressed inhibition of *ptc-lacZ* expression by (J and N) *mago RNAi* but (K and O) not by *Srp54 RNAi*. (L and P) Maximal *ptc-lacZ* intensity as a percentage of controls for *fu*; *Su(fu)*/+ wing discs expressing *mago* and *Srp54* RNAi, with or without a *gCi* transgene, showing means and 95% C.I.s for $n = 4$ experiments. (Q and R) Loss of one copy of *ci* (R) reduced *ptc-lacZ* (red) expression in *fu*; *Su(fu)*/+ wing discs. (S–V) MARCM clones (marked by GFP, green) that lose a second chromosome *gCi* transgene in wing discs that are ci^{94}/+ and either (S and T) include a third chromosome *gCi* transgene or (U and V) express *UAS-Ci* with *C765-GAL4*. (S and U) Ci-155 levels (white) were increased greatly by *UAS-Ci* expression but were not affected by exchange of *gCi* transgenes. (T and V) Only excess Ci-155 from *UAS-Ci* decreased *ptc-lacZ* (red) and anterior En (white) expression at the AP border (yellow arrows). AP, anterior/posterior; En, engrailed; Hh, Hedgehog; Ptc, Patched; RNAi, RNA interference; wt, wild-type.

Ci-155 processing in the absence of PKA, so the reduced levels of Ci-155 likely represent a lower rate of Ci-155 production, consistent with the observation that Srp54 RNAi reduced *ci* RNA levels (Figure 3).

The additional effect of Srp54 RNAi reducing the rate of Ci-155 processing, inferred from elevated anterior Ci-155 in otherwise normal wing discs (Figure 2, J, L, and N), can explain the different impacts of Mago and Srp54 in different clones. Hh target gene activation appears to be more sensitive to reductions in Ci-155 levels in *GAP-Fu* clones than in *pka* clones based on the stronger effect of Mago inhibition in *GAP-Fu* clones. However, the reduction of Ci-155 levels expected from *Srp54 RNAi* lowering *ci* RNA is substantially offset in *GAP-Fu* clones (and not at all in *pka* clones) because *Srp54 RNAi* additionally reduces Ci-155 processing only in the *GAP-Fu* clones. Hence, *Srp54 RNAi* barely inhibits *ptc-lacZ* in *GAP-Fu* clones, whereas *ptc-lacZ* inhibition in *pka* clones is greater than for *mago RNAi*, probably because *Srp54 RNAi* causes a larger reduction in *ci* RNA (Figure 3). Altogether, clonal analyses are consistent with the hypotheses that both Mago and Srp54 inhibition reduce Hh pathway activity by reducing *ci* RNA levels, and that Srp54 inhibition also impairs Ci-155 processing.

Effects of Ci-155 levels on Hh pathway activity

We next explored whether reduced levels of Ci-155 primary translation product, inferred from studies of *ci* RNA and Ci-155 antibody staining, could plausibly explain the alterations in Hh pathway activity seen in response to inhibition of Mago and Srp54. In a *fu*; *Su(fu)*/+ background, heterozygosity for *Srp54* (in *Df(2L)BSC240*), *mago*, or *Y14* reduced v3–4 spacing. Normal spacing was restored by a single copy of a 16-kb *ci* genomic transgene (Methot and Basler 1999) inserted at an

Table 1 Rescue to adulthood of ci^{94}/ci^{94} null flies by *gCi* transgenes

	transgene/+; ci^{94}/ci^{94} (% *transgene/+; ci^{94}/+*)	*transgene/transgene; ci^{94}/ ci^{94}* (% *transgene/+; ci^{94}/+*)
gCi	49 (*n = 298*)	94 (*n = 1052*)
gCi ATG-B	83 (*n = 550*)	99 (*n = 530*)
gCi ATG-A	0 (*n > 300*)	0 (*n > 300*)
SV-1	23 (*n = 699*)	75 (*n = 350*)
Ci-1	0 (*n = 298*)	9 (*n = 603*)

att site on chromosome 3 ("*gCi*") (Figure 5, A–H). In the same genetic background (*fu*; *Su(fu)/+*), addition of the *gCi* transgene enhanced *ptc-lacZ* expression (Figure 5, I, L, and M), while heterozygosity for *ci* reduced *ptc-lacZ* expression (Figure 5, Q and R). Thus, reduced *ci* gene dosage can phenocopy the effects of reduced Mago or Srp54 activity and an extra *ci* transgene can suppress heterozygous Mago and Srp54 phenotypes, consistent with Mago and Srp54 acting through regulation of *ci* RNA levels.

When Mago activity was reduced more drastically using RNAi in *fu*; *Su(fu)/+* discs, adding the *gCi* transgene substantially restored *ptc-lacZ* expression (Figure 5, J, L, and N), consistent with Mago acting solely by modifying *ci* RNA levels. However, analogous complementation was not observed for *Srp54 RNAi* (Figure 5, K, O, and P), suggesting that severe reduction in Srp54 activity does not act solely by reducing *ci* RNA.

The effect of excess Ci on Hh signaling was tested by expressing a *UAS-Ci cDNA* transgene using *C765-GAL4* in MARCM clones at the AP border. Ci-155 levels were greatly elevated in clones and induced strong *ptc-lacZ* expression in posterior clones, as expected due to stimulation by Hh (Smelkinson *et al.* 2007), but did not induce *ptc-lacZ* in anterior clones (Figure 5, S–V). Surprisingly, clones at the AP border showed reduced expression of both *ptc-lacZ* and En (Figure 5V), whereas control clones had no such changes (Figure 5T), implying that excess Ci-155 can impair Hh signaling. Thus, small reductions in Ci-155 primary translation product can reduce Hh pathway activity under sensitized conditions, while excess Ci-155 can impair normal Hh signaling.

ci-A and ci-B RNA encode similar Ci activator functions

The confirmed existence of *ci-B* RNA in wing discs, albeit at much lower levels than *ci-A* RNA, as well as the potential for Mago to regulate the relative levels of *ci-A* and *ci-B* (Figure 3), led us to question the functional role of *ci-B* RNA. The *ci-B* RNA does not include the first coding exon of *ci-A* and it would be expected to encode a translation product that initiates at M119 of the Ci-A protein (Figure 3A). Therefore, we constructed two variants of the *gCi* transgene, in which the expected initiation codons for either Ci-A (*gCi ATG-A*) or Ci-B (*gCi ATG-B*) were altered to AAG Lys codons.

We found that *gCi ATG-B* (lacking Ci-B) rescued *ci* null (ci^{94}) flies to adulthood with a similar efficiency to *gCi WT* (Table 1); the profile of *ptc-lacZ* expression and Ci-155 protein of rescued wing discs was also very similar (Figure 6, A–D), suggesting that Ci-B protein has no essential function under normal conditions. It remains possible that *ci-B* RNA has a function independent of protein products or that it encodes a protein initiating downstream of M119 that substitutes for Ci-B function when M119 is altered.

Neither one nor two copies of *gCi ATG-A* rescued any *ci* null animals to adulthood (Table 1), but rescue to third larval instar was observed. Wing discs from those animals showed reduced levels of AP border *ptc-lacZ* and Ci-155, together with enlarged anterior compartments (Figure 6, E–H). Ci-B (the sole expected product of *gCi ATG-A*) may have little or no Ci-75 repressor function based on the prior observation of loss of repressor activity for a Ci variant lacking residues 6–339 (Zhou and Kalderon 2010). Loss of Ci repressor leads to ectopic *dpp* induction in anterior cells and anterior expansion (Methot and Basler 1999). Consistent with the possibility that Ci-B defects stem largely from the failure to produce a repressor, *gCi ATG-A* was able to rescue adult flies transheterozygous for ci^{94} and the ci^{Ce} allele, which produces only a Ci repressor that is not regulated by Hh (Methot and Basler 1999) (Table 2). Rescue of ci^{Ce}/ci^{94} animals by a single copy of *gCi ATG-A* was less efficient than for *gCi WT* and resulted in more severe narrowing of the v3–4 interval, but both shortcomings were largely rectified by providing two copies of the transgene (Figure 6, O–V and Table 2). These properties suggest that *gCi ATG-A* generates a Ci activator that is regulated normally but present at slightly reduced levels, most likely because of less efficient use of the Ci-B translation initiation codon compared to Ci-A, or perhaps reduced stability of Ci-B protein compared to Ci-A.

Properties of intronless ci transgenes

It is possible that regulation of the efficiency of *ci-A* RNA splicing, or even a regulatory role of *ci-B* RNA independent of Ci-B protein production, are important for Hh signaling. To test these ideas, we constructed two *gCi* transgene variants, in which all intron sequences had been removed. One variant (*Ci-1*) retained the normal *ci* 3′-UTR sequences, while the other (*SV-1*) instead included 3′-UTR sequences from Simian Virus 40, with the expectation that this 3′-UTR, commonly employed for high-level gene expression, might enhance protein translation (Figure 6I).

Ci-1 rescued *ci* null adults only when present in two copies, and very inefficiently, while *SV-1* had rescue activity intermediate between *Ci-1* and *gCi WT* (Table 1). Ci-155 protein levels encoded by *Ci-1* were much lower than for

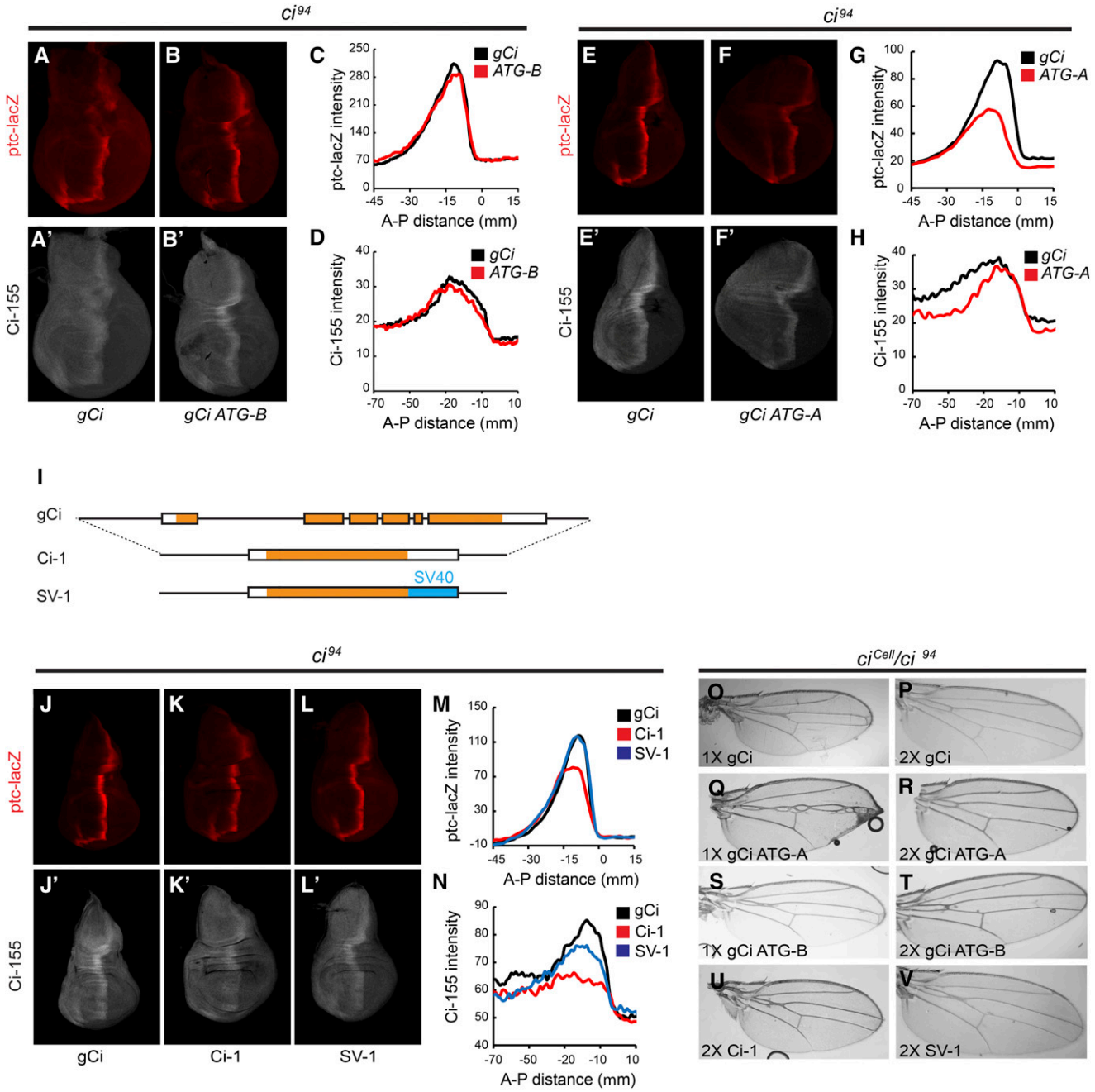

Figure 6 Activities of Ci-A, Ci-B proteins, and intronless *ci* transgenes. (A, B, H, and F) Wing discs from *ci* null larvae with a *gCi* transgene that (A and E) is wild-type, or lacks the initiator codon for (B) Ci-B or (F) Ci-A, stained for *ptc-lacZ* (red) or Ci-155 (white). (C and G) *ptc-lacZ* and (D and H) Ci-155 intensity profiles along the AP axis for single experiments ($n = 4$ wing discs). (I) Diagram representing the structure of *gCi*, *Ci-1*, and *SV-1* transgenes, in which introns are deleted (boxed regions are exons with coding sequence in orange). In *SV-1*, the 3′-UTR was replaced by SV40 3′-UTR sequences (blue). (J–L) *ci* null wing discs with one copy of (J) *gCi*, (K) *Ci-1*, or (L) *SV-1*, stained for *ptc-lacZ* (red) and Ci-155 (white). (M) *ptc-lacZ* and (N) Ci-155 intensity profiles along the AP axis for single experiments ($n = 3$ wing discs). (O–V) Wings from ci^{Cell}/ci^{94} flies with one copy or two copies of (O and P) *gCi*, (Q and R) *gCi ATG-A*, (S and T) *gCi ATG-B*, (U) *Ci-1*, or (V) *SV-1*. AP, anterior/posterior.

gCi WT, while *SV-1* Ci-155 levels were only marginally lower (Figure 6, J'–L', and N). We were not able to collect enough rescued wing discs to measure *ci* RNA to determine if intron removal in *Ci-1* reduced Ci-155 protein because of reduced transcription, RNA stability, or translation. AP border expression of *ptc-lacZ* appeared normal in discs rescued by *SV-1* but was slightly reduced in the very few wing discs rescued by *Ci-1* (Figure 6, J–M).

Rescue of ci^{Ce}/ci^{94} animals showed a similar pattern. *Ci-1* produced almost no adults, even when present in two copies, and did not support the normal v3–4 spacing endowed by two copies of *gCi WT* (Figure 6U and Table 2). *SV-1* rescued

Table 2 Rescue to adulthood of ci^{Cell}/ci^{94} flies by *gCi* transgenes

	transgene/+; ci^{Ce}/ci^{94} (% *transgene/+*; $ci^{94}/+$)	*transgene/transgene*; ci^{Ce}/ci^{94} (% *transgene/+*; $ci^{94}/+$)
gCi	44 (*n* = 218)	76 (*n* = 992)
gCi ATG-B	20 (*n* = 208)	92 (*n* = 286)
gCi ATG-A	17 (*n* = 440)	32 (*n* = 462)
SV-1	0 (*n* = 192)	21 (*n* = 843)
Ci-1	0 (*n* = 546)	0 (*n* = 941)

no adults in one copy but in two copies rescue approached the efficiency of one copy of *gCi WT*, with a modest wing vein abnormality (Figure 6V and Table 2).

These results show that *ci* introns are important to support normal functional levels of Ci-155 and provide further evidence that relatively small reductions in Ci-155 levels compromise robust Hh signaling (measured by rescue efficiency and phenotypes) in a number of settings, including reduced *ci* gene dosage or the presence of constitutive Ci repressor.

The functional deficit of *Ci-1* relative to *SV-1* is likely due to reduced Ci-155 levels and *SV-1* undoubtedly has considerable ability to support Hh signaling. However, the surprisingly poor rescue of ci^{Ce} animals by *SV-1*, given almost normal Ci-155 levels, suggests that intron removal may also compromise some regulatory input from Hh.

ci RNA as a direct target of Mago and Srp54 function in Hh signaling

The significant, though incomplete, rescue activity of the *SV-1* transgene provided a way to test whether Mago or Srp54 acted directly on *ci* RNA splicing to impact Hh signaling. If so, we should see no effect of Mago or Srp54 inhibition on signaling through *SV-1*. We were able to test this most effectively in the context of *pka* mutant clones, where both *mago RNAi* and *Srp54 RNAi* reduced *ptc-lacZ* induction in otherwise wild-type wing discs (Figure 4, H–K, N, and O). When a single copy of the *gCi WT* transgene rescues a *ci* null, ectopic *ptc-lacZ* expression in *pka* mutant clones was much lower than in wild-type discs and not satisfactory for testing the effects of Mago and Srp54 inhibition (data not shown). However, *ptc-lacZ* expression could be increased to an intermediate level by using either a heterozygous *Su(fu)* background (Figure 7A) or two copies of the transgene (Figure 7K).

The level of *ptc-lacZ* induced in *pka* mutant clones in *Su(fu)/+* flies with one copy of *gCi WT* (and otherwise *ci* null) was reduced ~25% by expression of *mago RNAi* (Figure 7, A, B, and I). *SV-1* supported a slightly lower level of *ptc-lacZ* induction than *gCi WT*, consistent with lower Ci-155 levels produced by *SV-1*, but *mago RNAi* produced no change (Figure 7, C, D, and I). Similarly, Ci-155 levels were reduced at the AP border of wing discs by *mago RNAi* for *gCi* but not *SV-1* (Figure 7, E–H, and J). These results are consistent with *mago RNAi* normally reducing Hh pathway activity by reducing the levels of the major spliced *ci* RNA (*ci-A*) and primary Ci-155 translation product.

The level of *ptc-lacZ* induced in *pka* mutant clones by two copies of *gCi WT* (and otherwise *ci* null) was reduced almost 20% by expression of *Srp54 RNAi* (Figure 7, K, L, and S). *SV-1* supported a lower level of *ptc-lacZ* induction and *Srp54 RNAi* produced no reduction in *ptc-lacZ* expression in the presence of only *SV-1* (Figure 7, M, N, and S). This result is consistent with *Srp54 RNAi* normally reducing Hh pathway activity in *pka* mutant clones by reducing the levels of spliced *ci* RNA.

Srp54 RNAi, in contrast to *mago RNAi*, inhibited Hh signaling in wild-type wing discs, suggesting that this action may not be mediated by reducing *ci* RNA levels (Figure 2, A–F). Indeed, we found that *Srp54 RNAi* still decreased *ptc-lacZ* expression at the AP border of wing discs expressing only *SV-1* (Figure 7, O–R and T). Elevated anterior Ci-155 in response to *Srp54 RNAi* was also evident in the presence of *SV-1*, confirming that this action of Srp54 is also not dependent on *ci* splicing (Figure 7, O'–R'). Thus, Srp54 affects *ci* RNA splicing slightly differently to Mago but with the same functional consequence of reducing *ci-A* RNA levels, leading to lowered rates of Ci-155 production and Hh pathway deficits in several settings, including *pka* mutant clones. Srp54 additionally, through currently uncharacterized mechanisms, appears to promote Ci-155 processing in anterior cells and Hh signaling at the AP border.

Discussion

We used a genetic modifier screen to identify new components in Hh signal transduction. Surprisingly, the screen identified EJC components and an SR protein, all with established functions in regulating RNA. Further investigation revealed *ci* RNA as a direct target and clarified the roles of different *ci* RNAs and the levels of their primary translation products in Hh signaling (Figure 8).

Direct actions of Mago and Srp54 that impact Hh signaling

Reducing the level of each of the core EJC components, Mago, Y14, and eIF4AIII, reduced Hh pathway activity under sensitized conditions, while inhibition of Btz did not affect Hh signaling. This pattern of EJC contributions has been observed previously for the archetypal studies showing EJC regulation of splicing of *MAPK* and *piwi* (Ashton-Beaucage *et al.* 2010; Roignant and Treisman 2010; Hayashi *et al.* 2014; Malone *et al.* 2014), and therefore suggested that RNA splicing may be the relevant EJC focus in Hh signaling. We found that loss of Mago reduced Hh pathway activity cell autonomously in *pka* mutant clones and in clones expressing activated Fu, indicating an effect on Hh signal transduction. Mago inhibition did not affect Hh signaling when mediated by a *ci* transgene (*SV-1*) that contained no introns, identifying *ci* RNA splicing as

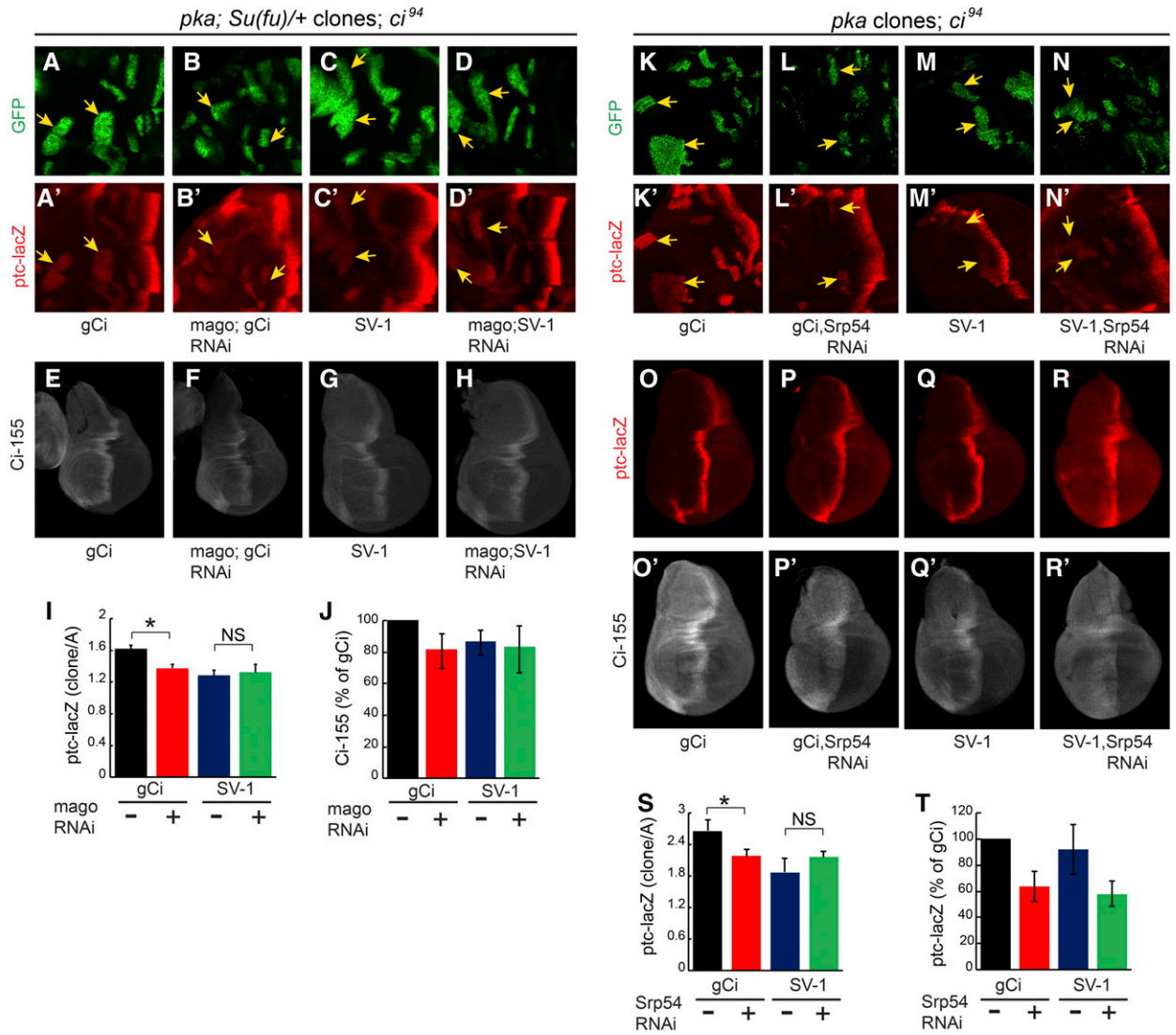

Figure 7 An intronless *ci* transgene tests *ci* RNA splicing as a key target of Mago and Srp54. (A–D and K–N) Ectopic *ptc-lacZ* (red) induced in anterior *pka* clones (marked by GFP, green, arrows) in wing discs null for *ci* with (A–D) one copy of a *ci* transgene and heterozygous for *Su(fu)* or (K–N) two copies of a *ci* transgene, was measured in the presence or absence of (A–D) *mago RNAi* or (K–N) *Srp54 RNAi*. (A, C, K, and M) *ptc-lacZ* expression was higher for discs with *gCi* than for *SV-1* and was reduced by *mago RNAi* and *Srp54 RNAi* (A, B, K, and L) in the presence of *gCi* but (C, D, M, and N) not in the presence of *SV-1*. (I and S) *ptc-lacZ* expression in *pka* clones in discs of the designated genotypes relative to discs with *gCi* (and no RNAi), showing mean, SEM, and significant differences by Student's *t*-test (* $P < 0.05$) for (I) $n = 3$, $n = 3$, $n = 4$, and $n = 3$ clones, and (S) $n = 11$, $n = 9$, $n = 7$, and $n = 12$ clones in the order shown. (E–H) Ci-155 (white) in *ci* null wing discs with two copies of *gCi* or *SV-1* in the presence or absence of *mago RNAi* expression. (J) Maximal Ci-155 intensity as a percentage of wing discs with *gCi*, showing means and 95% C.I.s from two independent experiments of $n = 6$ discs for each condition. Ci-155 levels were reduced by Mago inhibition for *gCi* but not for *SV-1*. (O–R and T) *ptc-lacZ* (red) and Ci-155 (white) in *ci* null wing discs expressing *UAS-Diap1* with two copies of *gCi* or *SV-1* in the presence or absence of *Srp54 RNAi*. (T) Maximal *ptc-lacZ* intensity at the AP border as a percentage of wing discs with *gCi*, showing means and 95% C.I.s from two independent experiments of $n = 6$ discs for each condition. AP, anterior/posterior; RNAi, RNA interference.

the key Mago target. We also observed changes in the pattern of *ci* RNAs when Mago was inhibited. Specifically, the level of a minor alternatively spliced product (*ci-B*) was increased while the level of the major splice form (*ci-A*) was decreased by an amount commensurate with observed reductions in Ci-155 protein levels and Hh target gene inhibition (Figure 8).

The evidence for Srp54 acting directly on *ci* RNA splicing is similar to that for Mago in terms of cell autonomous action and a failure to influence Hh pathway activity when the only source of Ci protein is an RNA (from the *SV-1* transgene) that does not need to be spliced. However, unlike Mago depletion, inhibition of Srp54 reduced the levels of *ci* RNA measured across most introns but did not alter the ratio of *ci-A* and *ci-B* RNAs, so it is unlikely that Srp54 is acting on *ci* RNA in concert with EJC components, despite some evidence of association of Srp54 with EJCs in directing alternative splicing (Sakashita *et al.* 2004).

For Srp54, unlike Mago, we also found evidence for effects on the Hh pathway that are not mediated by alterations in *ci* RNA. First, Ci-155 protein was increased in anterior wing disc cells when Srp54 was inhibited (Figure 8). This most likely

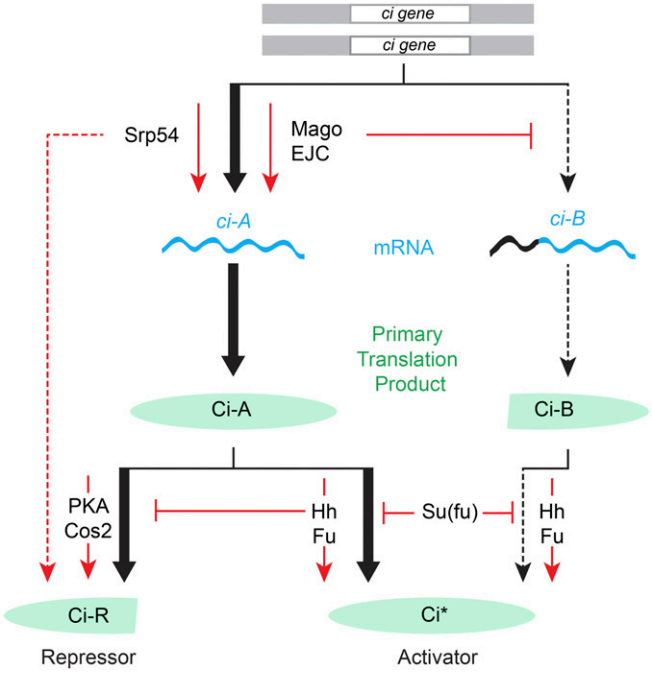

Figure 8 Role of the EJC, Srp54, and *ci* RNA production in Hh signal transduction. In the absence of Hh, full-length Ci-155 protein is largely inactive and processed slowly, with the participation of PKA and Cos2, into active Ci-75 repressor. Hh signal transduction via activation of Smo leads to inhibition of Ci-155 processing, leading to a loss of Ci-75 repressor and a greater accumulation of Ci-155 primary translation product. Hh also promotes activation of Ci-155 via Fu kinase and in opposition to Su(fu). Activated Ci-155 is subject to Cul3-mediated degradation (data not shown). The role of Ci-155 levels in contributing to Hh target gene activation is not well-studied. Here, we have found that reduced rates of Ci-155 production due to reduced *ci* gene dose, genetic removal of *ci* intronic sequences, or reduced production of the major *ci* RNA (*ci-A*) through inhibition of core nuclear EJC factors or Srp54, reduce Hh pathway activity under conditions of submaximal activation (by Hh in the absence of Fu kinase, by synthetic Fu activation, or by loss of PKA or Cos2). Loss of Su(fu), like reduced Ci-155 production, only affects Hh pathway activity under an overlapping set of conditions for submaximal pathway activation, illustrating the potential for partial redundancy in regulating Ci-155 levels and Ci-155 activity. The minor *ci-B* RNA is increased in the absence of Mago and encodes a protein with normally regulated activator function but appears not to be processed to a functional repressor. EJC, exon junction complex; Fu, Fused; Hh, Hedgehog; PKA, Protein kinase A; Smo, Smoothened; Su(fu), Suppressor of fused.

reflects impaired Ci-155 proteolytic processing to Ci-75 repressor because Srp54 inhibition actually lowered Ci-155 levels when Ci-155 processing was eliminated in *pka* mutant clones. Second, Srp54 inhibition reduced *ptc-lacZ* induction at the AP border of normal wing discs, whereas twofold reduction in *ci* dosage or Mago inhibition had no effect. Moreover, AP border *ptc-lacZ* inhibition was not rescued by providing excess *ci* and it was still observed when the only source of *ci* was an intronless transgene. Thus, Srp54 has additional uncharacterized actions that impinge on Hh signaling.

Ci-155 protein levels in Hh signaling

It has previously been recognized that Hh signaling alters both the amounts and activities of Ci proteins (Briscoe and Therond 2013). However, the impact of regulating Ci-155 levels has not yet been investigated carefully. In this study, we have altered the rate of production of the primary full-length Ci translation product through heterozygosity for *ci*, various *ci* transgenes, and Mago inhibition. We consistently observed that Hh pathway activity was altered by twofold or lesser changes in Ci-155 levels under conditions where normal Hh signaling was compromised (loss of Fu kinase) or only partially phenocopied (by loss of *pka* or synthetic Fu activation). The observed sensitivity to relatively small changes in Ci-155 makes it plausible that any mechanism that regulates Ci-155 levels, including regulation of *ci* splicing, contributes to normal Hh signaling (Figure 8).

Impact of alternative ci RNAs and ci splicing on Hh signal transduction

Our observation that Mago inhibition altered the proportion of *ci-A* and *ci-B* RNA prompted investigation of potentially distinctive roles of these RNAs. Both public data and our investigation of wing disc RNA showed *ci-B* to be much less abundant than *ci-A*. Hence, we first considered the hypothesis that *ci-B* might encode a hyperactive form of Ci activator, potentially induced as a feed-forward mechanism to achieve the highest levels of Hh signaling. Our investigations did not support that speculation. A *ci* transgene lacking the initiator codon for Ci-B supported normal Hh signaling, while another transgene lacking the initiation codon for Ci-A, and therefore expected to produce more Ci-B protein than normal, was not hyperactive. Instead, the *gCi ATG-A* transgene product appeared to be a normally regulated activator that does not generate an active processed repressor. At present, we cannot therefore assign a distinct function to the N-terminally truncated protein that is predicted to be encoded by *ci-B* RNA.

We additionally tested the properties of two *ci* transgenes lacking any intronic sequences. *SV-1*, which included an *SV40* 3′-UTR in place of *ci* sequences, produced significantly more Ci-155 protein than *Ci-1* and had greater rescue activity in the absence of normal *ci* gene activity. Both were less active than a wild-type transgene but exhibited improved function in two doses. The dose-dependent and graded deficiencies of these transgenes provide further evidence of the importance of the levels of Ci-155 primary translation product for Hh signaling. We did not determine why intron removal reduced Ci-155 production, but two plausible possibilities are that the large first intron includes a transcriptional enhancer or that translation efficiency is compromised, as observed for some other genes following intron removal (Chorev and Carmel 2012). Although substantially reduced Ci-155 levels provide a sufficient explanation for major deficits of *Ci-1*, the rescue activity of *SV-1*, most notably in a ci^{Ce} background, was lower than expected from measurements of Ci-155 levels. This quantitative limitation of the activity of an intronless transgene suggests that the presence of introns in *ci* may also serve a regulatory role that is important for *ci* to transduce Hh signals robustly.

When assessing the impact of a regulatory process in Hh signaling, it is important to consider the potential for partially or fully redundant mechanisms (Figure 8). Su(fu) provides a notable example of a factor that is central to the mechanism of Hh signal transduction in *Drosophila* and mammals, but only discernibly affects Hh pathway activity in *Drosophila* under conditions that perturb normal Hh signaling (Preat 1992; Zhou and Kalderon 2011). In fact, Mago affects Hh pathway activity under exactly the same conditions as Su(fu) (*e.g.*, in *pka* mutant clones or when Fu kinase is inactive) but not under normal conditions (Figure 8). Similarly, deficiencies of intronless *ci* transgenes are especially evident under sensitized conditions (reduced *ci* dosage, *pka* mutant clones, or in the presence of a constitutive repressor). To resolve the contribution of potentially regulated *ci* splicing, the EJC, Srp54, and translatable *ci* RNA levels to Hh signaling, it will be necessary to simultaneously eliminate regulation through Ci-155 activation, Ci-155 processing, and Ci-155 proteolysis individually, and perhaps in combination. At present, the studies described here have alerted us to the possibility that *ci* RNA transcription and processing, the EJC, and an SR protein splicing factor may all play a significant role in regulating the output of Hh signaling.

Acknowledgments

We thank the Bloomington *Drosophila* Stock Center, the Vienna *Drosophila* Resource Center, the Developmental Studies Hybridoma Bank, Jessica Treisman, and Alain Vincent for fly stocks and antibodies; Sarah Finkelstein, Allyson Ray, Jessica Chan, Hana Littleford, and Maryam Mudasir for assistance with experiments; and Jessica Treisman, Jose F. de Celis, and Amy Reilein for discussions. This work was supported by the National Institutes of Health (grant GM-041815). The authors declare no competing or financial interests.

Author contributions: E.G.G., J.C.L., and D.K. were responsible for conceptualization and methodology; E.G.G., J.C.L., and D.K. for formal analysis and investigation; E.G.G. and D.K. for writing (original draft preparation); E.G.G., J.C.L., and D.K. for reviewing and editing the manuscript; E.G.G. and J.C.L. for visualization; and D.K. for funding acquisition.

Literature Cited

Amoyel, M., and E. A. Bach, 2014 Cell competition: how to eliminate your neighbours. Development 141: 988–1000.

Anderson, E., S. Peluso, L. A. Lettice, and R. E. Hill, 2012 Human limb abnormalities caused by disruption of hedgehog signaling. Trends Genet. 28: 364–373.

Ashton-Beaucage, D., and M. Therrien, 2011 The exon junction complex: a splicing factor for long intron containing transcripts? Fly (Austin) 5: 224–233.

Ashton-Beaucage, D., C. M. Udell, H. Lavoie, C. Baril, M. Lefrancois *et al.*, 2010 The exon junction complex controls the splicing of MAPK and other long intron-containing transcripts in Drosophila. Cell 143: 251–262.

Blair, S. S., 2007 Wing vein patterning in Drosophila and the analysis of intercellular signaling. Annu. Rev. Cell Dev. Biol. 23: 293–319.

Bradley, T., M. E. Cook, and M. Blanchette, 2015 SR proteins control a complex network of RNA-processing events. RNA 21: 75–92.

Briscoe, J., and P. P. Therond, 2013 The mechanisms of Hedgehog signalling and its roles in development and disease. Nat. Rev. Mol. Cell Biol. 14: 416–429.

Chorev, M., and L. Carmel, 2012 The function of introns. Front. Genet. 3: 55.

Claret, S., M. Sanial, and A. Plessis, 2007 Evidence for a novel feedback loop in the Hedgehog pathway involving smoothened and fused. Curr. Biol. 17: 1326–1333.

Dietzl, G., D. Chen, F. Schnorrer, K. C. Su, Y. Barinova *et al.*, 2007 A genome-wide transgenic RNAi library for conditional gene inactivation in Drosophila. Nature 448: 151–156.

Han, Y., Q. Shi, and J. Jiang, 2015 Multisite interaction with Sufu regulates Ci/Gli activity through distinct mechanisms in Hh signal transduction. Proc. Natl. Acad. Sci. USA 112: 6383–6388.

Hayashi, R., D. Handler, D. Ish-Horowicz, and J. Brennecke, 2014 The exon junction complex is required for definition and excision of neighboring introns in Drosophila. Genes Dev. 28: 1772–1785.

Herold, N., C. L. Will, E. Wolf, B. Kastner, H. Urlaub *et al.*, 2009 Conservation of the protein composition and electron microscopy structure of Drosophila melanogaster and human spliceosomal complexes. Mol. Cell. Biol. 29: 281–301.

Hui, C. C., and S. Angers, 2011 Gli proteins in development and disease. Annu. Rev. Cell Dev. Biol. 27: 513–537.

Humke, E. W., K. V. Dorn, L. Milenkovic, M. P. Scott, and R. Rohatgi, 2010 The output of Hedgehog signaling is controlled by the dynamic association between suppressor of fused and the Gli proteins. Genes Dev. 24: 670–682.

Kennedy, C. F., A. Kramer, and S. M. Berget, 1998 A role for SRp54 during intron bridging of small introns with pyrimidine tracts upstream of the branch point. Mol. Cell. Biol. 18: 5425–5434.

Kent, D., E. W. Bush, and J. E. Hooper, 2006 Roadkill attenuates Hedgehog responses through degradation of Cubitus interruptus. Development 133: 2001–2010.

Le Hir, H., J. Sauliere, and Z. Wang, 2016 The exon junction complex as a node of post-transcriptional networks. Nat. Rev. Mol. Cell Biol. 17: 41–54.

Lee, T., and L. Luo, 2001 Mosaic analysis with a repressible cell marker (MARCM) for Drosophila neural development. Trends Neurosci. 24: 251–254 (erratum: Trends Neurosci. 24: 385).

Malone, C. D., C. Mestdagh, J. Akhtar, N. Kreim, P. Deinhard *et al.*, 2014 The exon junction complex controls transposable element activity by ensuring faithful splicing of the piwi transcript. Genes Dev. 28: 1786–1799.

Methot, N., and K. Basler, 1999 Hedgehog controls limb development by regulating the activities of distinct transcriptional activator and repressor forms of Cubitus interruptus. Cell 96: 819–831.

Oh, S., M. Kato, C. Zhang, Y. Guo, and P. A. Beachy, 2015 A comparison of Ci/Gli activity as regulated by Sufu in Drosophila and mammalian Hedgehog response. PLoS One 10: e0135804.

Ohlmeyer, J. T., and D. Kalderon, 1998 Hedgehog stimulates maturation of Cubitus interruptus into a labile transcriptional activator. Nature 396: 749–753.

Organista, M. F., M. Martin, J. M. de Celis, R. Barrio, A. Lopez-Varea *et al.*, 2015 The Spalt transcription factors generate the transcriptional landscape of the Drosophila melanogaster wing pouch central region. PLoS Genet. 11: e1005370.

Pak, E., and R. A. Segal, 2016 Hedgehog signal transduction: key players, oncogenic drivers, and cancer therapy. Dev. Cell 38: 333–344.

Park, J. W., K. Parisky, A. M. Celotto, R. A. Reenan, and B. R. Graveley, 2004 Identification of alternative splicing regulators

by RNA interference in Drosophila. Proc. Natl. Acad. Sci. USA 101: 15974–15979.
Petrova, R., and A. L. Joyner, 2014 Roles for Hedgehog signaling in adult organ homeostasis and repair. Development 141: 3445–3457.
Preat, T., 1992 Characterization of suppressor of fused, a complete suppressor of the fused segment polarity gene of Drosophila melanogaster. Genetics 132: 725–736.
Roignant, J. Y., and J. E. Treisman, 2010 Exon junction complex subunits are required to splice Drosophila MAP kinase, a large heterochromatic gene. Cell 143: 238–250.
Ryder, E., M. Ashburner, R. Bautista-Llacer, J. Drummond, J. Webster *et al.*, 2007 The DrosDel deletion collection: a Drosophila genomewide chromosomal deficiency resource. Genetics 177: 615–629.
Sakashita, E., S. Tatsumi, D. Werner, H. Endo, and A. Mayeda, 2004 Human RNPS1 and its associated factors: a versatile alternative pre-mRNA splicing regulator in vivo. Mol. Cell. Biol. 24: 1174–1187.
Smelkinson, M. G., Q. Zhou, and D. Kalderon, 2007 Regulation of Ci-SCFSlimb binding, Ci proteolysis, and hedgehog pathway activity by Ci phosphorylation. Dev. Cell 13: 481–495.
Tukachinsky, H., L. V. Lopez, and A. Salic, 2010 A mechanism for vertebrate Hedgehog signaling: recruitment to cilia and dissociation of SuFu-Gli protein complexes. J. Cell Biol. 191: 415–428.
Vervoort, M., 2000 Hedgehog and wing development in Drosophila: a morphogen at work? Bioessays 22: 460–468.
Wu, J. Y., A. Kar, D. Kuo, B. Yu, and N. Havlioglu, 2006 SRp54 (SFRS11), a regulator for tau exon 10 alternative splicing identified by an expression cloning strategy. Mol. Cell. Biol. 26: 6739–6747.
Xiong, Y., C. Liu, and Y. Zhao, 2015 Decoding Ci: from partial degradation to inhibition. Dev. Growth Differ. 57: 98–108.
Zhang, Q., L. Zhang, B. Wang, C. Y. Ou, C. T. Chien *et al.*, 2006 A hedgehog-induced BTB protein modulates hedgehog signaling by degrading Ci/Gli transcription factor. Dev. Cell 10: 719–729.
Zhang, Z., L. Shen, K. Law, Z. Zhang, X. Liu *et al.*, 2016 Suppressor of fused chaperones Gli proteins to generate transcriptional responses to Sonic Hedgehog signaling. Mol. Cell. Biol. 37: e00421-16.
Zhou, Q., and D. Kalderon, 2010 Costal 2 interactions with Cubitus interruptus (Ci) underlying Hedgehog-regulated Ci processing. Dev. Biol. 348: 47–57.
Zhou, Q., and D. Kalderon, 2011 Hedgehog activates fused through phosphorylation to elicit a full spectrum of pathway responses. Dev. Cell 20: 802–814.

Communicating editor: N. Perrimon